CellPress
OPEN ACCESS

Trends in
Biotechnology

Research Article

# Regulatable C-X-C chemokine receptor type 4 in iPSC-derived NK cells improves bone marrow chemotaxis and targeting resident tumor

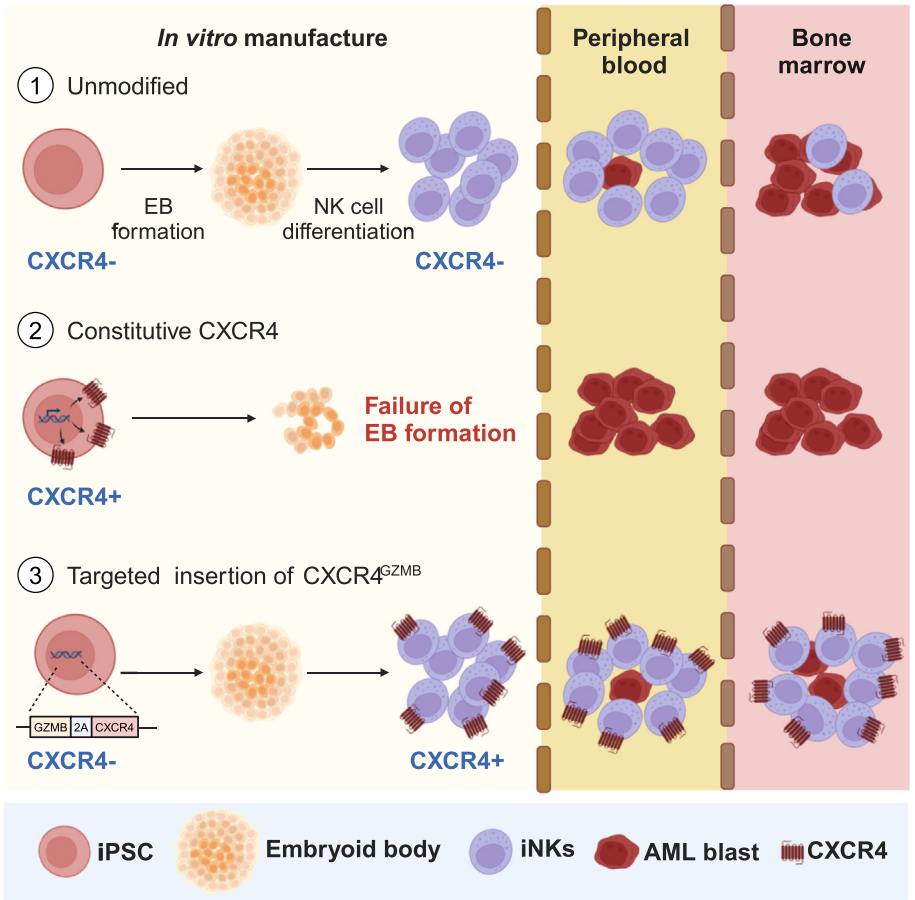


In this study, He *et al*. developed an optimized method that combines iPSC differentiation, chemotaxis regulation, and genetic engineering to produce a potential iPSC-derived nature killer cells product with enhanced therapeutic efficacy against bone marrow-resident tumors, such as acute myeloid leukemia and multiple myeloma.

Xiangjun He (何向军), Linqin Wang (王林钦), Wenxiu Zeng (曾文秀), Yiyun Wang (王艺芸), Nian Chen (陈念), Peng Yang (杨鹏), Aijun Ti (提爱军), Qi Zhang (张琦), Yuxuan Shao (邵雨轩), Mengyan Wang (王梦岩), Zihan Huang (黄子函), Xueyan Zhang (张雪燕), Mengqi Xu (许梦绮), Lingmin Liang (梁灵敏), Xinye Wang (汪昕晔), Xiaohui Ding (丁晓辉), Tingting Zhu (朱婷婷), Peng Zhang (张朋), Ziyi Pan (潘梓怡), Fei Yang (杨菲), Yixuan Zhou (周怡璇), Guolong Mo (莫国龙), Jiabiao Hu (胡嘉彪), Yanan Yue (岳亚男), Jiapan Hu (胡佳盼), Yujie Deng (邓玉杰), Tony Ho, George M. Church, Yongxian Hu (胡永仙), He Huang (黄河), Luhan Yang (杨璐菡)
xiangjun.he@qihanbio.com (X. He),
huanghe@zju.edu.cn (H. Huang)
luhan.yang@qihanbio.com (L. Yang).

## Highlights

Relapsed or refractory acute myeloid leukemia (R/R AML) characterized by aberrant myeloid cell production in the bone marrow (BM) was challenged by a lack of potent therapeutics.

Human iPSC-derived nature killer cells (iNKs), as a potent cellular therapy for R/R AML, show limited BM infiltration due to low expression of the BM homing chemokine receptor (C-X-C chemokine receptor type 4, CXCR4).

While engineering iPSC with high CXCR4 expression hampers its differentiation to hematopoietic stem cells, this limitation can be circumvented by regulatable CXCR4 expression at the iNK stage through genetic engineering.

CXCR4-iNKs exhibit improved cytotoxicity against BM-resident tumors, and this efficacy could be further augmented by the incorporation of chimeric antigen receptor targeting AML antigens.

Trends in Biotechnology, July 2025,
Vol. 43, No. 7
https://doi.org/10.1016/j.tibtech.2025.02.018

Trends in Biotechnology

CellPress OPEN ACCESS

Research Article

# Regulatable C-X-C chemokine receptor type 4 in iPSC-derived NK cells improves bone marrow chemotaxis and targeting resident tumor

Xiangjun He (何向军)[1,8,*], Linqin Wang (王林钦)[2,8], Wenxiu Zeng (曾文秀)[1,8], Yiyun Wang (王艺芸)[3,8], Nian Chen (陈念)[1], Peng Yang (杨鹏)[1], Aijun Ti (提爱军)[1], Qi Zhang (张琦)[1], Yuxuan Shao (邵雨轩)[1], Mengyan Wang (王梦岩)[1], Zihan Huang (黄子函)[3], Xueyan Zhang (张雪燕)[4], Mengqi Xu (许梦绮)[1], Lingmin Liang (梁灵敏)[1], Xinye Wang (汪昕晔)[1], Xiaohui Ding (丁晓辉)[1], Tingting Zhu (朱婷婷)[1], Peng Zhang (张朋)[1], Ziyi Pan (潘梓怡)[1], Fei Yang (杨菲)[1], Yixuan Zhou (周怡璇)[1], Guolong Mo (莫国龙)[1], Jiabiao Hu (胡嘉彪)[1], Yanan Yue (岳亚男)[1], Jiapan Hu (胡佳盼)[1], Yujie Deng (邓玉杰)[5], Tony Ho[6], George M. Church[7], Yongxian Hu (胡永仙)[2], He Huang (黄河)[2,*], and Luhan Yang (杨璐菡)[1,*]

**iPSC-derived natural killer cells (iNKs) have emerged as a promising cellular therapy, especially for the refractory or relapsed acute myeloid leukemia (R/R AML) patients, but limited research focused on the chemotaxis of iNKs. Here we demonstrate that C-X-C chemokine receptor type 4 (CXCR4) is significantly reduced in iNKs, resulting in impaired bone marrow (BM) infiltration, which cannot be rescued by constitutively expressed CXCR4 in iPSC due to CXCR4-induced differentiation failure. To address this, we developed a strategy to allow specific expression of CXCR4 during the iNK maturation stage without compromising the final iNK yield and function. The engineered iNKs exhibited enhanced BM infiltration, resulting in improved therapeutic effects in AML murine models. This, brought attention to iNK chemotaxis, provided a meaningful strategy by incorporating well-designed gene editing with stem cells for cell product development, and obtained improved effective NK cells for AML therapy.**

## Introduction

AML is a clonal HSC malignancy characterized by the accumulation of immature myeloid blasts with arrested differentiation, leading to the suppression of normal hematopoiesis [1]. Current treatment regimens include combination chemotherapy, the use of hypomethylating agents, and/or HSC transplantation [2]. However, most patients ultimately relapse and fail with these standard-of-care therapies [3]. Patients with relapsed or refractory AML (R/R AML) have a poor prognosis, with a median overall survival (OS) of only 6 months and a 5-year OS rate of 10% [4]. Consequently, potent therapeutics for R/R AML are highly demanded.

**Chimeric antigen receptor** (see Glossary) T (CAR-T) cell therapy represents a significant advancement in cancer treatment, particularly for R/R B cell malignancies [5]. Recently, CAR-T cells have been employed in the treatment of R/R AML, demonstrating efficacy against drug-resistant leukemia cells bearing multiple genetic mutations [6–8]. However, there has yet to be a significant breakthrough in clinical trials for AML treatment due to the inherent heterogeneity

## Technology readiness

iPSCs provide an ideal resource for generating immune cells, with well-established methodologies enabling the derivation of diverse cell types, including natural killer (NK) cells (iNKs). These iNKs have exhibited cytotoxicity against a range of cancers, including both hematologic and solid malignancies, thereby presenting a promising approach for cell-based therapies. In this study, we integrated iNK differentiation with CRISPR-based gene editing to develop cell products with enhanced antitumor functionality. This technology has currently achieved Technology Readiness Level (TRL) 5, indicating it is feasible to advance to clinical trials.

Specifically, the expression of CXCR4 was challenged by its effect on hematopoietic stem cell (HSC) differentiation, which resulted in limited infiltration of final iNKs into bone marrow. Through precise genetic engineering techniques, we established a regulatable gene expression system to mitigate potential adverse effects during the differentiation process. This study underscores the importance of *in vivo* distribution and chemotaxis profiling in the development of cell-based product, highlighting the need for the optimization of manufacturing processes.

of AML cell populations [9]. Furthermore, the manufacturing failure of autologous CAR-T cell products is frequently observed in patients with AML who have undergone extensive lines of chemotherapy. Therefore, the development of universal cellular products with improved function is imperative for advancing R/R AML therapy.

**Natural killer cells (NKs)** are innate lymphoid cells capable of eliminating tumor cells via various underlying mechanisms, including the secretion of cytotoxic molecules and ligand-induced target cell apoptosis [10]. Notably, the infusion of allogeneic NKs does not induce **graft-versus-host disease**, rendering them suitable candidates for the development of universal cell products. Recent studies have indicated that **iPSC**-NK cells (iNKs) exhibit potent cytotoxicity against a wide range cancers, including both hematologic and solid malignancies. Human iPSC armored with various functional modules through genetic engineering can be isolated and further expanded as a homogeneous cell bank to produce stable iNK products, rendering them attractive cell sources for AML therapy [11–14].

Despite numerous studies focused on enhancing the antitumor activity of iNKs, there has been limited investigation into their *in vivo* chemotaxis. Accumulating evidence indicates that the homing ability of CAR-T or CAR-NK cells to the **BM microenvironment** is a prerequisite for mediating consistent therapeutic activity in AML [15]. The trafficking of lymphocytes into the BM primarily depends on the expression of CXCR4, a chemokine receptor that binds to CXCL12, which is highly expressed by stromal and endothelial cells in the BM [16,17]. CXCR4 expression changes dynamically during hematopoiesis, endowing cells at various differentiation stages with distinct retention and homing capability [18]. Meanwhile, it has been found that culture conditions can attenuate the expression of chemokine receptors, potentially impairing their homing ability to the BM [19]. Consequently, the BM chemotaxis of iNKs requires further exploration, particularly concerning the role of CXCR4 in the differentiation process of iPSC into NKs.

In this study, we observed limited BM infiltration of iNKs and identified a significant reduction in CXCR4 gene expression compared with peripheral blood NK cells (PBNKs). We transduced CXCR4 into iNKs using **lentivirus**, which markedly improved their BM infiltration in murine models. However, iPSCs with constitutive CXCR4 expression failed to differentiate into hematopoietic cells, as evidenced by differentiation failure and the absence of $CXCR4^{+}$ iNKs obtained. Transcriptomic analysis revealed that CXCR4 impacts iPSC-to-HSC differentiation by impeding mesoderm/HSC formation and reducing proliferative capacity. To circumvent the differentiation limitations induced by CXCR4, we utilized the **CRISPR/Cas9** system to knock-in CXCR4 at the granzyme B (GZMB) locus and obtained stable iPSC clones for differentiation. This approach enables the specific expression of CXCR4 during the iNK maturation stage without compromising the yield and functional capacity of the final iNK products. The CXCR4-enhanced iNKs exhibited a marked enhancement in BM infiltration capabilities, thereby ameliorating therapeutic effects in AML murine models. Overall, our findings underscore the critical role of CXCR4 in mediating iNK BM chemotaxis and provide a strategic approach involving proper genetic engineering to enhance the therapeutic effects of iNKs in the treatment of AML.

## Results

### CXCR4 augmented the iPSC-derived NK cell BM infiltration

To monitor the biodistribution of iNKs *in vivo*, we generated IL15-iNKs derived from iPSCs with exogenous expression of the IL15Rα-IL15 fusion protein to enhance persistency (see Figures S1A–C and Table S1 in the supplemental information online). We investigated the distribution of IL15-iNKs in a NOG murine model and observed that the iNKs initially aggregated in the lungs within the first 24 h and subsequently redistributed to other organs on day 7, with high

[1]Qihan Bio Inc., Hangzhou, Zhejiang, China
[2]Bone Marrow Transplantation Center of The First Affiliated Hospital & Liangzhu Laboratory, Zhejiang University School of Medicine, Hangzhou, Zhejiang, China
[3]Institute of Immunology and Department of Rheumatology, Sir Run Run Shaw Hospital, Zhejiang University School of Medicine, Hangzhou, Zhejiang, China
[4]Women's Hospital, Zhejiang University School of Medicine, Hangzhou, Zhejiang, China
[5]Life Sciences Institute, Zhejiang University, Hangzhou, Zhejiang, China
[6]Johns Hopkins University Hospital, Department of Neurology, Baltimore, MD, USA
[7]Department of Genetics, Harvard Medical School, Boston, MA, USA
[8]These authors contributed equally

*Correspondence:
xiangjun.he@qihanbio.com (X. He), huanghe@zju.edu.cn (H. Huang), and luhan.yang@qihanbio.com (L. Yang).

concentrations observed in the spleen, lungs, stomach, and liver. Unexpectedly, we observed limited distribution of IL15-iNKs in the BM, the target organ for AML therapy, where blast cells exist (Figure S1D in the supplemental information online).

To further elucidate this observation, we profiled the expression of chemotactic receptor in iNKs and IL15-iNKs, comparing them with PBNKs. Notably, we found that CXCR4, a crucial receptor for immune cell BM trafficking, exhibited significantly lower expression in iNKs and IL15-iNKs at the RNA and protein levels (Figure 1A,B and Table S2). Subsequently, we transduced IL15-iNKs with CXCR4 or luciferase (as control) using lentivirus, then infused the iNKs into NOG mice for pharmacokinetic (PK) analysis (Figure 1C). Expectedly, we observed a significant increase in the number of CXCR4 overexpressed IL15-iNKs homing to the BM compared with their control group at post-day 14 ($P < 0.001$), with a comparable cell number in peripheral blood (PB) (Figure 1D). Thus, we concluded that IL15-iNKs exhibit defective CXCR4 expression, resulting in compromised BM homing, which can be rescued by ectopic expression of CXCR4, offering a promising approach for AML therapeutics.

### CXCR4 expression affected hematopoietic differentiation of iPSC

To rescue the BM homing of iNKs, we engineered iPSC to stably express CXCR4. Based on the level of CXCR4 expression, we generated and separated the edited iPSC clones into two distinct groups: $CXCR4^{low}$ and $CXCR4^{high}$ (Figure 2A). Meanwhile, the unedited iPSC clones were used as a control group to monitor differentiation. There was no significant difference in cell morphology among these three groups of iPSC clones (Figure S2A). However, we observed a slight decrease of stemness in the $CXCR4^{high}$ group, as indicated by the expression of pluripotency markers (Figure S2B).

Unexpectedly, all iPSC clones within the $CXCR4^{high}$ group failed to form **embryoid bodies (EBs)**, indicating that high level of CXCR4 expression inhibits hematopoietic differentiation (Figure 2C, right panel). By contrast, iPSC clones in the $CXCR4^{low}$ group showed normal EB formation with CD34 expression levels comparable with the control group [Figure 2C (middle panel) and D]. By the end of iNK differentiation, we observed the typical NK cell phenotype characterized by the expression of CD56 and CD45 in the $CXCR4^{low}$ group (Figure S2C). However, the $CXCR4^{low}$ group exhibited relatively lower NK cell yields compared with the control group (Figure 2E). Importantly, subsequent detection of CXCR4 in differentiated iNKs revealed only a minimal number of cells expressing marginal CXCR4 (Figure 2F). Meanwhile, no significant difference was observed in the cytotoxic capability of the two types of iNKs against the AML cell line THP-1 (Figure 2G). These findings, suggest that high level of CXCR4 impedes the iPSC-to-NK differentiation process, potentially due to its impact on the hematopoietic stage, as corroborated by previous studies [20].

### Constitutive CXCR4 expression in iPSC caused defective HSC formation and expansion

To elucidate the underlying biological mechanism of CXCR4 impeding hematopoietic differentiation, both unedited control iPSC and $CXCR4^{high}$ iPSC clones were employed for HSC differentiation, with RNA-seq samples collected at differentiation day 0, 3, and 9 (Figure 3A). Notably, CXCL12 was constitutively highly expressed throughout the differentiation process, indicating an active CXCL12/CXCR4 axis in $CXCR4^{high}$ group (Figure 3B). **Principal component analysis (PCA)** showed that unedited control iPSC and $CXCR4^{high}$ iPSC clustered together at iPSC stage. However, as differentiation progressed, the $CXCR4^{high}$ group increasingly diverged from the control group (Figure 3C), especially at day 3 and 9. Notably, the $CXCR4^{high}$ D9 group was closer to the control D3 than to the control D9 group (Figure 3C).

To validate these findings, Venn diagram analysis was conducted, revealing a reduced number of differentially expressed genes (DEGs) in the control D3 versus $CXCR4^{high}$ D9 compared with

## Glossary

**Bone marrow microenvironment:** complex structure composed of a cellular compartment – including hematopoietic stem cells (HSCs), mesenchymal stromal cells, adipocytes, osteoblasts, osteoclasts, endothelial cells, macrophages, megakaryocytes, lymphocytes, neutrophils, and plasma cells – and a non-cellular compartment containing cytokines, chemokines, and growth factors. It plays a crucial role in maintaining hematopoietic homeostasis by regulating the self-renewal, proliferation, differentiation, and migration of HSCs and progenitor cells under normal conditions and in response to stress, infection, or injury.
**Chimeric antigen receptor (CAR):** recombinant receptor that combines antigen-binding and immune cell-activating functions, enabling the redirection of specificity and functionality in T lymphocytes and other immune cells.
**CRISPR/Cas9 system:** RNA-guided adaptive immune system in bacteria and archaea that has been adapted as one of the most efficient genome-editing tools. It can target a wide range of human genes and has potential applications in treating various diseases.
**Embryoid bodies (EBs):** self-organizing aggregates of PSCs that mimic certain aspects of early embryogenesis.
**Graft-versus-host disease:** immunological disorder occurring after allogeneic hematopoietic stem cell transplantation, which affects multiple organ systems, including the gastrointestinal tract, liver, skin, and lungs.
**Hematopoietic stem and progenitor cells (HSPCs):** rare, self-renewing, multipotent progenitors responsible for producing all types of blood cells through the process of hematopoiesis.
**iPSCs:** stem cells generated through the reprogramming of mature somatic cells by integrating specific transgenes into the genome. They exhibit properties of unlimited self-renewal and pluripotency.
**Lentivirus:** enveloped viruses belonging to the Retroviridae family that are widely used in biopharmaceutical applications due to their ability to stably integrate transgenes into both dividing and non-dividing cells.
**Natural killer cells (NKs):** innate immune effector cells capable of efficiently identifying and eliminating

control D3 versus CXCR4$^{high}$ D3 and control D9 versus CXCR4$^{high}$ D9, suggesting that CXCR4 expression delays iPSC hematopoiesis (Figure 3D). We further analyzed genes associated with pluripotency (GO:001982), mesoderm formation (GO:0007498), and hematopoiesis (GO:0030097). As shown in Figure 3E, the control group exhibited significant upregulation of mesoderm-related genes, while the CXCR4$^{high}$ group retained high levels of pluripotency markers at day 3. Similarly, by day 9, definitive HSCs were formed in the control group, whereas the CXCR4$^{high}$ group displayed signs of mesoderm formation rather than hematopoiesis.

Through KEGG analysis, we found that the CXCR4$^{high}$ group exhibited negative regulation of the cell cycle pathway at both day 3 and 9 (Figure 3F,G), potentially explaining the delayed hematopoiesis. In addition to cell cycle analysis, we performed gene ontology (GO) analysis on upregulated gene sets at EB day 3 and 9 for both control and CXCR4$^{high}$ groups. As shown in Figure 3H, upregulated genes in the control group were enriched for angiogenesis, vasculogenesis, and definitive hematopoiesis at day 3 of differentiation. By day 9, biological processes related to angiogenesis, blood vessel development, and lymph angiogenesis were enriched in the control group (Figure 3I), along with PI3K and MAPK pathways essential for immune cell development. However, no hematopoiesis-related developmental processes were detected in the CXCR4$^{high}$ group at either day 3 or day 9 (Figure 3H,I). Collectively, these findings demonstrate

abnormal cells, including virally infected cells and tumor cells.

**NKG2D ligand:** an activating receptor expressed by NK cells and certain T cell subsets. It serves as a major recognition receptor for detecting and eliminating cancer cells. Its ligands are stress-induced self-proteins that can also be secreted as soluble molecules via protease-mediated cleavage.

**Principal component analysis (PCA):** dimensionality reduction technique that simplifies complex datasets, enhancing interpretability while minimizing information loss.

**WHIM syndrome:** rare autosomal dominant immunodeficiency caused by gain-of-function mutations in the *CXCR4* gene. It is characterized by four key clinical features: warts, hypogammaglobulinemia, infections, and myelokathexis.

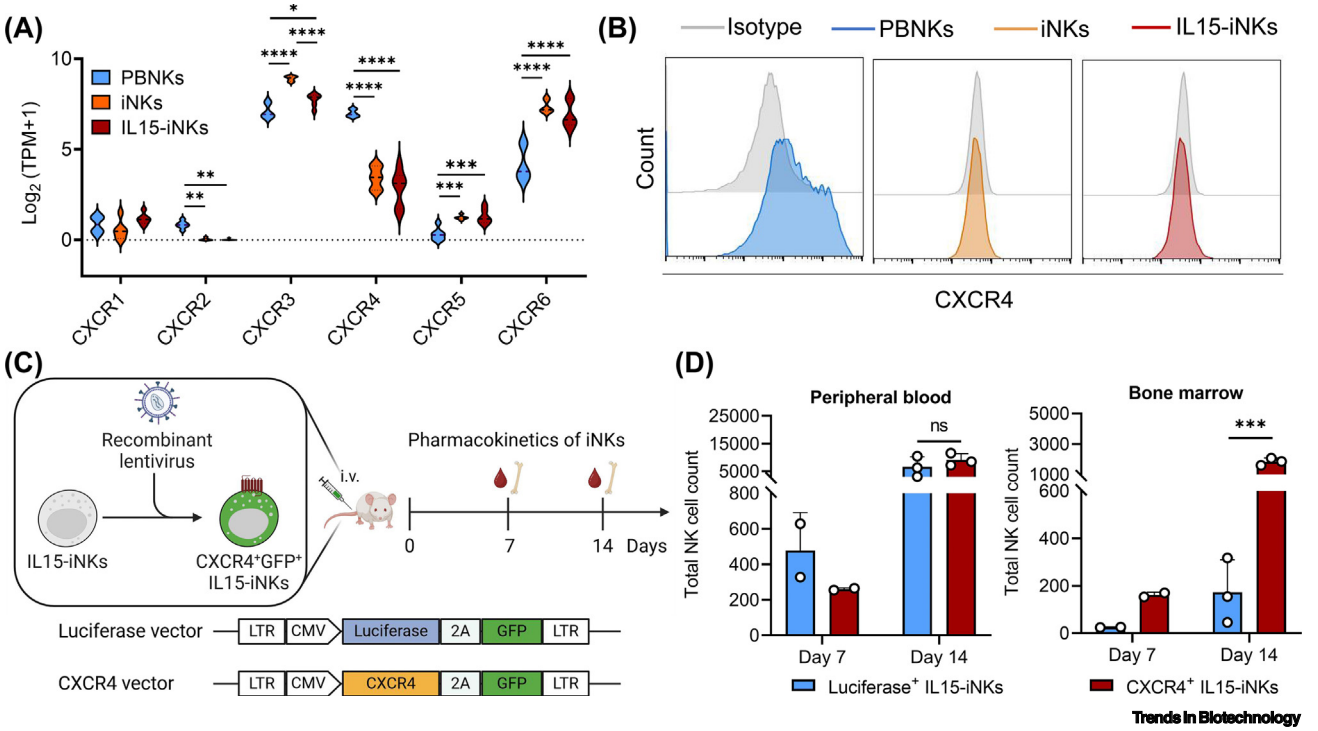


Figure 1. Limited bone marrow homing of IL15-iNKs could be rescued by overexpression of CXCR4. (A) RNA-seq reveals the transcriptional level of chemotaxis-associated genes in PBNKs, iNKs, and IL15-iNKs ($n$ = 6 for each group). Statistical significance was determined by one-way ANOVA or Kruskal-Wallis analysis, and Tukey test was used to analyze the specific difference group by group. (B) Flow cytometry analysis of CXCR4 expression on PBNKs, iNKs, and IL15-iNKs. (C) Experimental design to evaluate CXCR4 function in bone marrow (BM) homing using IL15-iNKs. IL15-iNKs were transduced with CXCR4 or luciferase (control), then infused into NOG mice for pharmacokinetic analysis ($n$ = 5 for each group). Two groups of mice were euthanized to obtain BM from femur at day 7 ($n$ = 2) and day 14 ($n$ = 3). BM was resuspended by 200 μl phosphate buffered saline (PBS) for further analysis. (D) Pharmacokinetics of iNKs by detecting CD45$^+$ CD56$^+$ cells in the same volume of peripheral blood (left) and BM (right) at day 7 and day 14 using flow cytometry. Statistical significance was determined by unpaired $t$ test. Data are presented as mean ± SD (D). *$P$<0.05, **$P$<0.01, ***$P$<0.001, ****$P$<0.0001; ns, no statistical significance. Abbreviations: CXCR4, C-X-C chemokine receptor type 4; iNK, iPSC-derived natural killer cell; PBNK, peripheral blood NK cell.

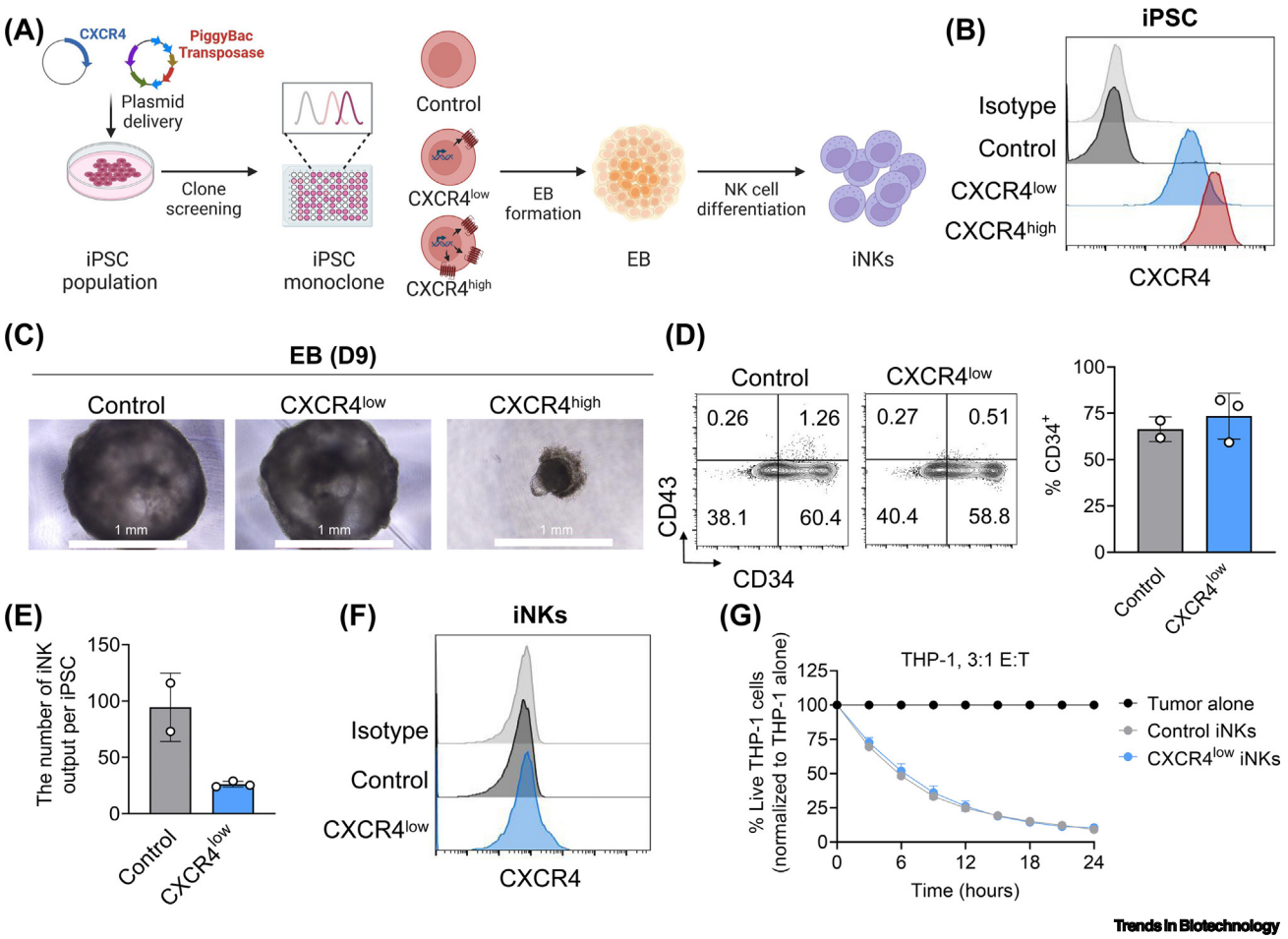


Figure 2. Overexpression of CXCR4 affects hematopoietic differentiation of iPSC. (A) Diagram of engineering iPSC with varying levels of CXCR4 expression and their iNK differentiation. (B) Flow cytometry analysis of CXCR4 expression on edited iPSC. (C) Representative images of embryoid bodies (EBs) formed by different iPSC groups at day 9. (D) Flow cytometry analysis of hematopoietic stem and progenitor cell (HSPC) markers (CD43 and CD34) on cells isolated from EB. The gating strategy was built to exclude the isotype staining strictly. (E) Final iNK ($CD56^+$) yields from $CXCR4^{low}$ iPSC clones ($n = 3$) and control iPSC clones ($n = 2$), demonstrated as final iNKs from each starting iPSC cell. (F) Flow cytometry analysis of CXCR4 levels on iNKs of different groups. (G) Cytotoxicity analysis of $CXCR4^{low}$ iNKs and control iNKs by targeting GFP-labeled THP-1 tumor cells at a 3:1 Effector-to-Target (E:T) ratio in an IncuCyte-based functional assay. Data are presented as mean ± SD (D,E,G). Abbreviations: CXCR4, C-X-C chemokine receptor type 4; iNK, iPSC-derived natural killer cell.

that CXCR4 affects iPSC-to-HSC differentiation by impeding mesoderm/HSC formation and reducing proliferative capacity.

## Successful CXCR4 expression in iPSC-differentiated NK cells through proper genetic engineering

Based on the aforementioned results, we proposed that engineering CXCR4 for specific activation during the NK stage could potentially overcome the differentiation barriers. We selected the GZMB locus as the target site due to its specific expression in iNKs with high transcript levels (Figure S3A and Table S3). As depicted in Figure 4A, we integrated CXCR4 directly behind the GZMB coding sequence, utilizing a 2A peptide to ensure proper expression. To monitor the transgene expression during the differentiation process, we established a control edited group with BFP as the transgene. Meanwhile, we employed the CRE-loxP system to facilitate efficient clone selection and subsequent removal of the selection gene cassette in the final iPSC clones. During the engineering process, we applied CRISPR/Cas9 for DNA double-strand break

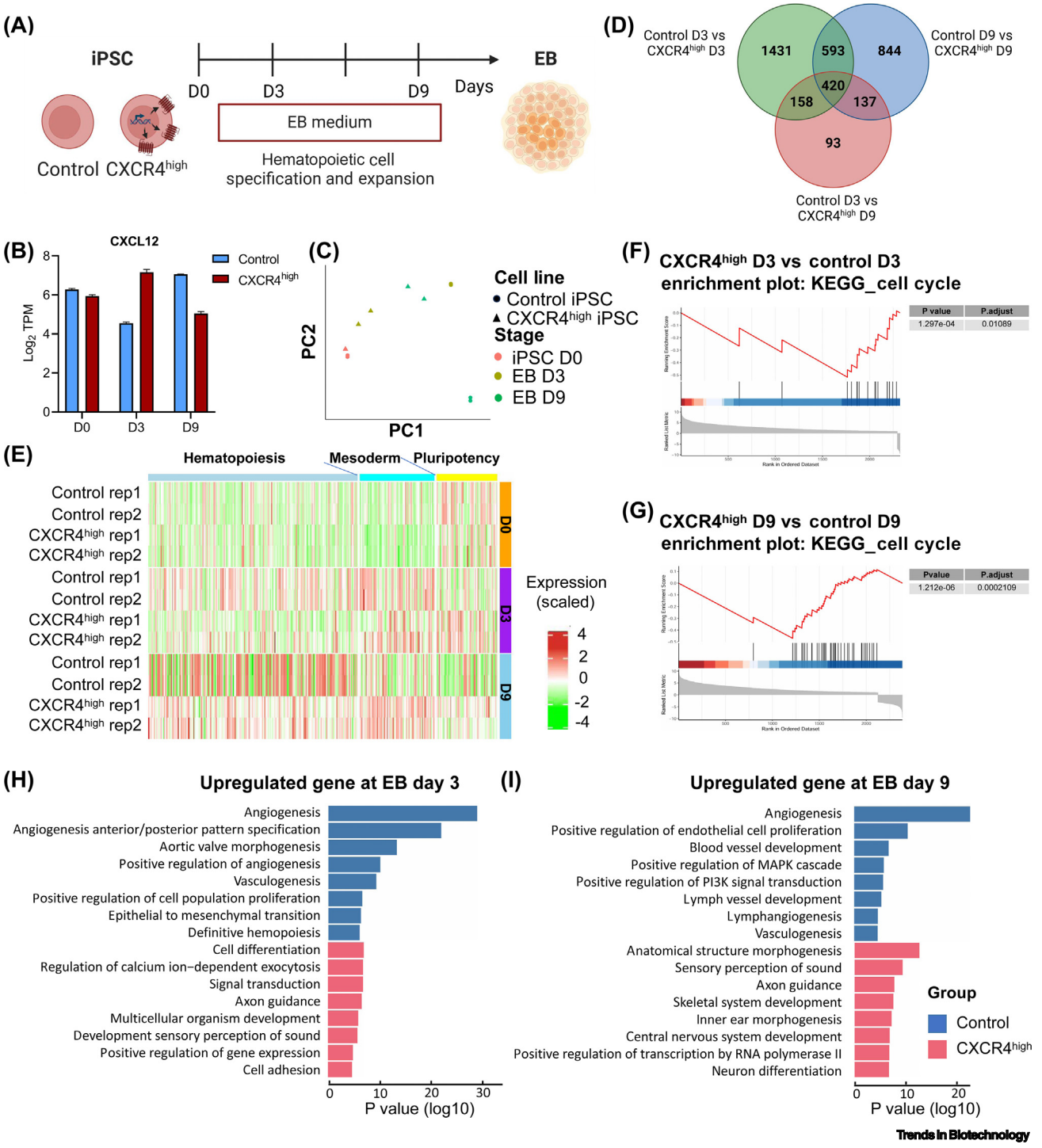


Figure 3. iPSCs with high CXCR4 expression fail in HSC specification. (A) Schematic of the HSC differentiation process. Control iPSCs and CXCR4$^{high}$ iPSCs were collected at day 0, 3, and 9 of EB formation for bulk RNA-seq analysis. (B) Expression levels of CXCL12 throughout HSC differentiation. (C) Principal component analysis (PCA) of all samples. (D) Venn diagram showing overlapping differentially expressed genes (DEGs) among comparisons: control D3 versus CXCR4$^{high}$ D3, control D9 versus CXCR4$^{high}$ D9, and control D3 versus CXCR4$^{high}$ D9. (E) Heatmap of gene expression related to pluripotency (GO:001982), mesoderm development

*(Figure legend continued at the bottom of the next page.)*

induction at the GZMB 3′ UTR locus, while concurrently providing a donor plasmid for repair. One week post-transfection, we isolated the stable integration iPSCs, identified by GFP positivity, and performed CRE transfection to excise the GFP-expressing element. Three days later, we sorted out the GFP-negative iPSCs for single clone expansion, followed by a rigorous screening process (Figures 4B and S3B in the supplemental information online). Finally, we obtained several clones, hereafter referred to as $CXCR4^{GZMB}$ and $BFP^{GZMB}$ clones, for differentiation (Figure S3C).

Prior to iNK differentiation, we confirmed that the transgene was not expressed at the iPSC stage (Figure S4A), and no abnormalities were observed in terms of iPSC morphology or pluripotency (Figure S4B). Both the $CXCR4^{GZMB}$ and the $BFP^{GZMB}$ groups successfully differentiated into **hematopoietic stem and progenitor cells (HSPCs)**, as indicated by $CD34^{+}$ expression at the EB stage (Figure 4C). At the end of iNK cell differentiation, the typical NK cell phenotype characterized by the expression of CD56 and CD45 was evident among all the groups (Figure S4C). Meanwhile, the $CXCR4^{GZMB}$ and $BFP^{GZMB}$ groups exhibited comparable iNK cell yield (Figure 4D) and expansion potential (Figure S4D). Most importantly, the transgene was successfully expressed in the final iNKs, without impact on the expression of CD94 and intracellular GZMB (Figure 4E). The $CXCR4^{GZMB}$ iNKs exhibited chemotaxis towards CXCL12 in a dose-dependent manner (Figure 4F), indicating the functionality of CXCR4 through this type of engineering approach.

In addition to assessing differentiation, we evaluated the cytolytic activity of the genetically modified iNKs against various tumor cell lines. In the killing assay, no significant difference was observed in cytotoxicity between $CXCR4^{GZMB}$ and $BFP^{GZMB}$ iNKs (Figure 4G), implying that CXCR4 expression would not affect NK cell cytotoxicity. Collectively, these findings suggest that the engineering process successfully achieved stable CXCR4 expression in iNKs without compromising iNK differentiation or cytotoxicity, therefore providing a promising strategy to improve the function of iNKs in AML therapy.

### $CXCR4^{GZMB}$ iPSC-derived NK cells show significant chemotaxis of BM and completely eradicate BM tumor cells

To investigate the potential *in vivo* therapeutic benefits of engineered iNKs expressing CXCR4 in treating AML, we assessed the efficacy of $CXCR4^{GZMB}$ iNKs in tumor-bearing NOG mice. THP-1, an AML tumor cell line capable of infiltrating BM (Figure S5A) and sensitive to iNKs due to high **NKG2D ligand** expression (Figure S5B,C), was selected as the tumor model for *in vivo* examination of $CXCR4^{GZMB}$ iNK cell function.

As illustrated in Figure 5A, on day –3, we injected $3 \times 10^5$ THP-1 cells expressing luciferase (THP-1-luc), followed by $5 \times 10^6$ $CXCR4^{GZMB}$ or $BFP^{GZMB}$ iNKs on day 0, 3, and 7 with imaging conducted on day 7, 9, 14, 17, and 21, respectively. Additionally, we dosed the mice with IL2 and IL15. Although iNK infusion reduced the tumor burden, the two groups did not exhibit a significant difference (Figure S6A,B), aligning with previous *in vitro* findings that CXCR4 did not enhance cytotoxicity (Figure 4G). Subsequently, we focused on tumor burden in BM to assess the benefit of CXCR4 expression. By day 21, femur samples were extracted for luminescent imaging and flow cytometry analysis, which revealed a significantly lower BM tumor burden in the $CXCR4^{GZMB}$ group compared with the $BFP^{GZMB}$ group (Figure 5B–D).

(GO:0007498), and hematopoiesis (GO:0030097). The bar on the left shows the range of scaled and centered log2 expression levels, with red indicating higher expression and green indicating lower expression. (F) Gene set enrichment analysis (GSEA) of KEGG cell cycle pathway using DEGs from $CXCR4^{high}$ D3 versus control D3. (G) GSEA of KEGG cell cycle pathway using DEGs from $CXCR4^{high}$ D9 versus control D9. (H,I) Gene ontology (GO) analysis of upregulated gene sets at EB day 3 and EB day 9 for both control and $CXCR4^{high}$ groups. Abbreviations: CXCR4, C-X-C chemokine receptor type 4; EB, embryoid body; HSC, hematopoietic stem cell; iNK, iPSC-derived natural killer cell stem.

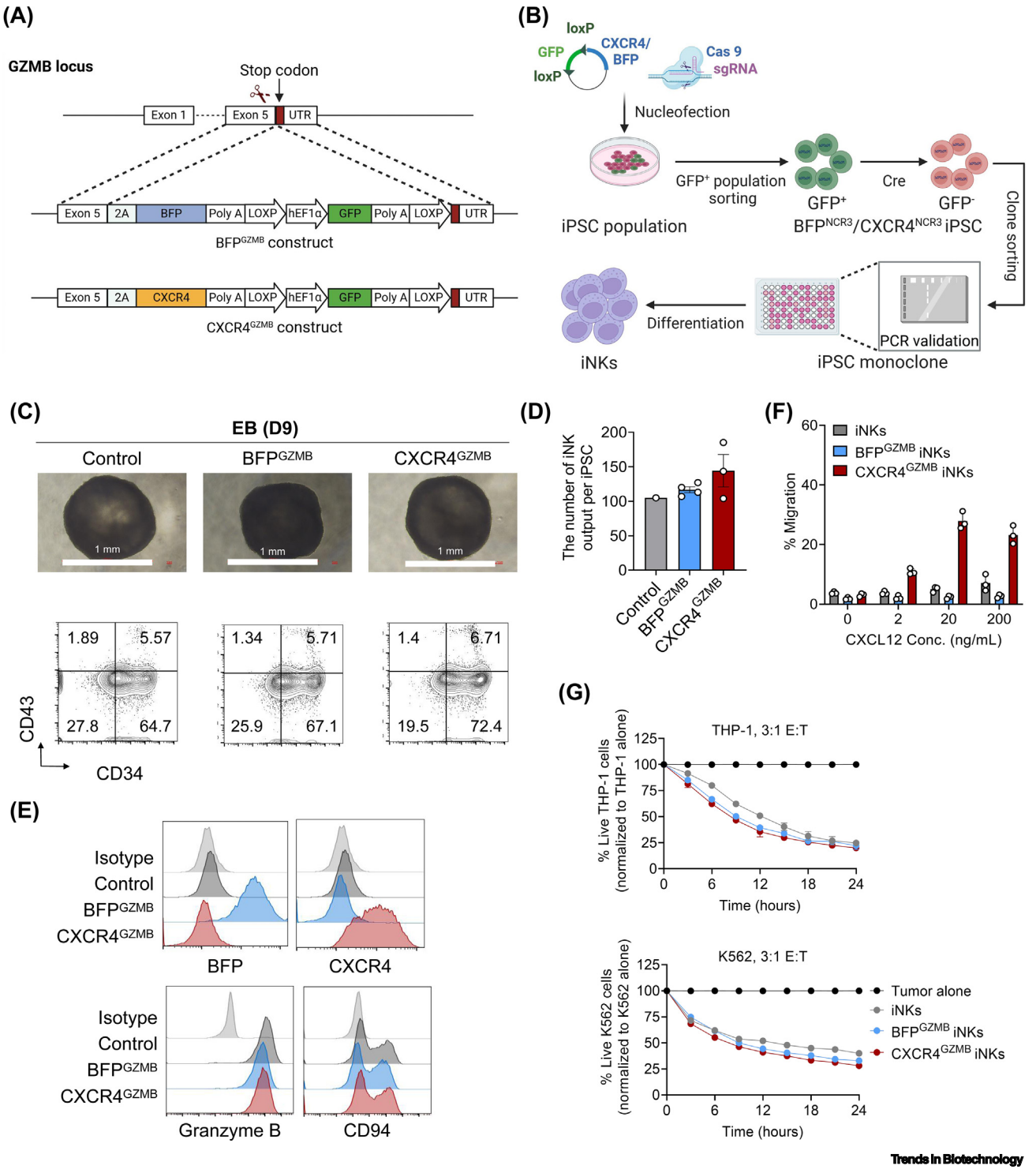


Figure 4. iPSC with targeted knock-in of CXCR4 at the GZMB locus demonstrate normal iNK differentiation and function. (A) Schematic view of targeted insertion of CXCR4 and *BFP* at GZMB locus. (B) Diagram illustrating the engineer process of $CXCR4^{GZMB}$ and $BFP^{GZMB}$ iPSC and their iNK differentiation process. (C) Representative images of EB formation of different groups of iPSC clones (upper panel). Flow cytometry analysis of hematopoietic stem and progenitor cell (HSPC)

*(Figure legend continued at the bottom of the next page.)*

In addition to tumor burden, we also analyzed the PK of iNKs in BM and PB. The number of iNKs in the BM of the CXCR4$^{GZMB}$ group was significantly higher than those in the BFP$^{GZMB}$ group by approximately 20-fold on both day 10 and 21 ($P < 0.01$, Figure 5E), but with comparable PK in PB. Through the cell cycle analysis, the superior *in vivo* efficacy of CXCR4$^{GZMB}$ iNKs is mediated by increased BM homing capability, not by IL15 and CXCL12 induced cell cycle change (Figure S6C).

Apart from the BM, we investigated the chemotaxis of CXCR4$^{GZMB}$ iNKs in other tissues. We employed digital droplet polymerase chain reaction (ddPCR) to detect CXCR4$^{GZMB}$ iNKs in various organs, including the lung, liver, heart, spleen, and kidney. We found that the CXCR4$^{GZMB}$ group demonstrated a significantly higher level of BM infiltration index than BFP$^{GZMB}$ group, while there was no significant difference in other organs (Figure 5F), implying a lower safety risk of enhanced CXCR4 expression.

### Incorporating CXCR4$^{GZMB}$ with CAR component enhances the therapeutic efficacy against AML

While previous studies have demonstrated the sensitivity of AML to NKs, the majority of AML cells remain refractory to NK cell-induced cytotoxicity due to intrinsic mechanisms. To further evaluate the potential therapeutic effects of CXCR4$^{GZMB}$, we armored iPSCs with CAR elements targeting prevalent AML antigens, including CD33 and CLL1. As illustrated in Figure S7A, we engineered iPSCs with aCD33-CAR and aCLL1-CAR, both with and without CXCR4$^{GZMB}$, and derived NK cells from these engineered iPSCs. The transgene was successfully expressed in the final iNKs, including aCD33-CAR, aCLL1-CAR, and CXCR4, respectively (Figure S7B). Furthermore, we conducted a killing assay targeting tumor cell lines with different expression patterns of CD33, CLL1, and NKG2D ligands, including K562, THP-1, and KG-1 (Figure S7C). All of these tumor cells secrete minimal CXCL12, excluding the possibility of CXCR4 chemotaxis affecting iNK function (Figure S7D). Consistent with previous findings that CXCR4 does not affect NK function, the CAR-iNKs exhibited similar killing abilities to CXCR4$^{+}$ CAR-iNKs against all tumor cells. However, CAR-iNKs, with or without CXCR4, showed enhanced cytotoxicity against KG-1 and THP-1 cells compared with iNKs, due to high CD33 and CLL1 expression (Figure S7E).

In addition to the *in vitro* assay, we further evaluated the *in vivo* function of CAR-iNKs with and without CXCR4$^{GZMB}$. We selected the KG-1 cell line as the tumor model due to its resistance to NK intrinsic killing and BM residence. We injected $2 \times 10^6$ KG-1 cells expressing luciferase (KG-1-luc), followed by $5 \times 10^6$ CAR-iNKs or CXCR4$^{+}$ CAR-iNKs on day 0, 3, and 7 with imaging conducted on days 0, 7, 10, 14, and 21, respectively. Additionally, we administered exogenous IL2 and IL15 to improve iNKs' *in vivo* persistence (Figure 6A). Although both iNK groups reduced the tumor burden, the CXCR4$^{+}$ CAR-iNKs demonstrated superior tumor eradication capabilities in both the whole body and the femur region (Figure 6B,C). By day 21, femur samples were extracted for flow cytometry analysis, revealing a significantly lower tumor burden and higher iNK cell number in the CXCR4$^{+}$ CAR-iNK group compared with the CAR-iNK group (Figure 6D). Statistical analysis showed a significant increase of the number of iNKs in the femur BM of the CXCR4$^{+}$ CAR-iNK group compared with the CAR-iNK group on day 21 ($P < 0.01$), with comparable PK in PB (Figure 6E). Moreover, the CXCR4$^{+}$ CAR-iNK demonstrated more potency in eliminating the KG-1 cells aggregating in lung ($P < 0.0001$, Figure 6F). All these data suggested that

markers (CD43 and CD34) on cells isolated from EBs at day 9 (lower panel). (D) Final iNK (CD56$^{+}$) yields at day 23 from CXCR4$^{GZMB}$ iPSC clones, BFP$^{GZMB}$ iPSC clones, and control iPSC clones, demonstrated as final iNKs from each starting iPSC. (E) Flow cytometry analysis of CXCR4, BFP, GZMB, and CD94 expression on iNKs derived from BFP$^{GZMB}$ and CXCR4$^{GZMB}$ iPSC clones. (F) *In vitro* migration of iNKs from upper chamber towards lower chamber with multiple concentrations (0, 2, 20, and 200 ng/ml) of CXCL12 through transwell assay, calculated by normalizing the number of iNKs in lower chamber to total iNKs. (G) Cytotoxicity of CXCR4$^{GZMB}$, BFP$^{GZMB}$, and control iNKs against GFP-labeled THP-1, and K562 tumor cells at a 3:1 Effector-to-Target (E:T) ratio in an IncuCyte-based functional assay. Data are presented as mean ± SD (D, F,G). Abbreviations: CXCR4, C-X-C chemokine receptor type 4; EB, embryoid body; GZMB, granzyme B; iNK, iPSC-derived natural killer cell.

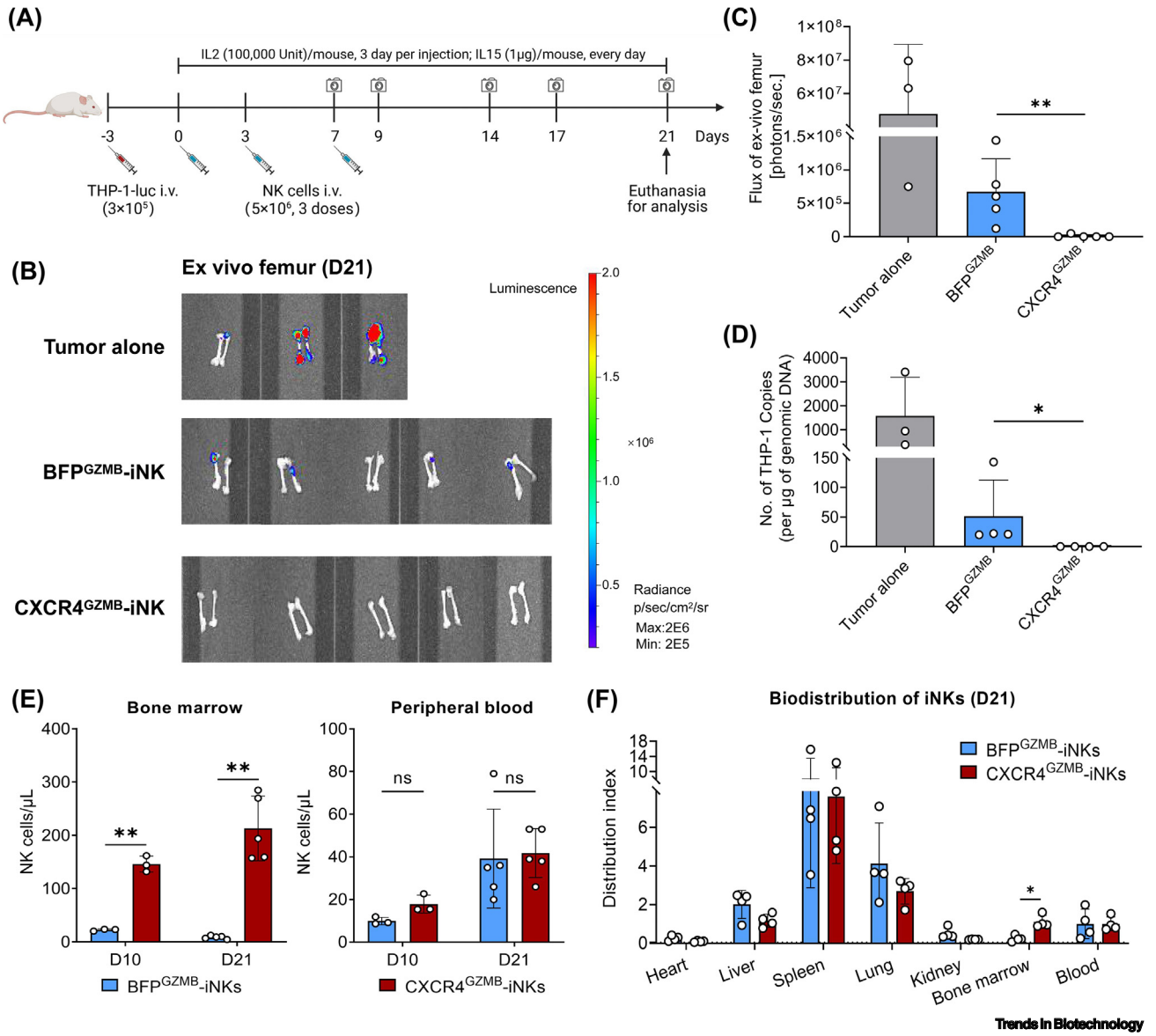


Figure 5. Regulatable CXCR4 in iPSC-derived NKs enhances BM homing and completely eradicates residual tumor in the BM. (A) Time schedule of *in vivo* functional evaluation of CXCR4$^{GZMB}$-iNKs using THP-1-luciferase xenograft models. (B) *Ex vivo* bioluminescence imaging of femur to evaluate tumor burden of each group in the THP-1-luciferase xenograft models. After tumor inoculation, mice, untreated ($n$ = 3), or treated with BFP$^{GZMB}$-iNKs ($n$ = 5) or CXCR4$^{GZMB}$-iNKs ($n$ = 5) were all euthanized at day 21 to obtain femurs. (C) Luminescence quantification of *ex vivo* femur shown in panel D. (D) Residual THP-1 cells in BM analyzed by droplet digital PCR (ddPCR). (E) Distribution of iNKs in PB and BM (obtained from femur) detected at day 10 and 21, respectively. Technically, the cells extracted from BM were resuspended in the same volume of PBS between BFP$^{GZMB}$-iNKs and CXCR4$^{GZMB}$ group. Left, Mann–Whitney *U* (D10) or unpaired *t* test (D21); right, unpaired *t* test with Welch's correction. (F) Biodistributions of CXCR4$^{GZMB}$-iNKs and BFP$^{GZMB}$-iNKs in various tissues, including heart, liver, spleen, lung, kidney, BM, and PB. 'Distribution index' was determined as tissue-infiltrated iNKs detected by ddPCR and then normalized to the levels in PB. Values are presented as mean ± SD (C–F). Analyses of differences between groups were performed using Mann–Whitney *U* test (C,D,F). $^{*}P<0.05$, $^{**}P<0.01$; ns, no statistical significance. Abbreviations: BM, bone marrow; CXCR4, C-X-C chemokine receptor type 4; GZMB, granzyme B; iNK, iPSC-derived natural killer cell; PB, peripheral blood.

engineering iNKs with aCD33-CAR and aCLL1-CAR significantly improves NK cytotoxicity against CD33$^{+}$ and/or CLL1$^{+}$ AML cells. Furthermore, we validate the migration potency and cytotoxicity of CXCR4$^{+}$ CAR-iNK in THP-1 murine model (Figure S8A,B). By day 20, femur samples were extracted for flow cytometry analysis, revealing a significantly lower tumor burden and higher

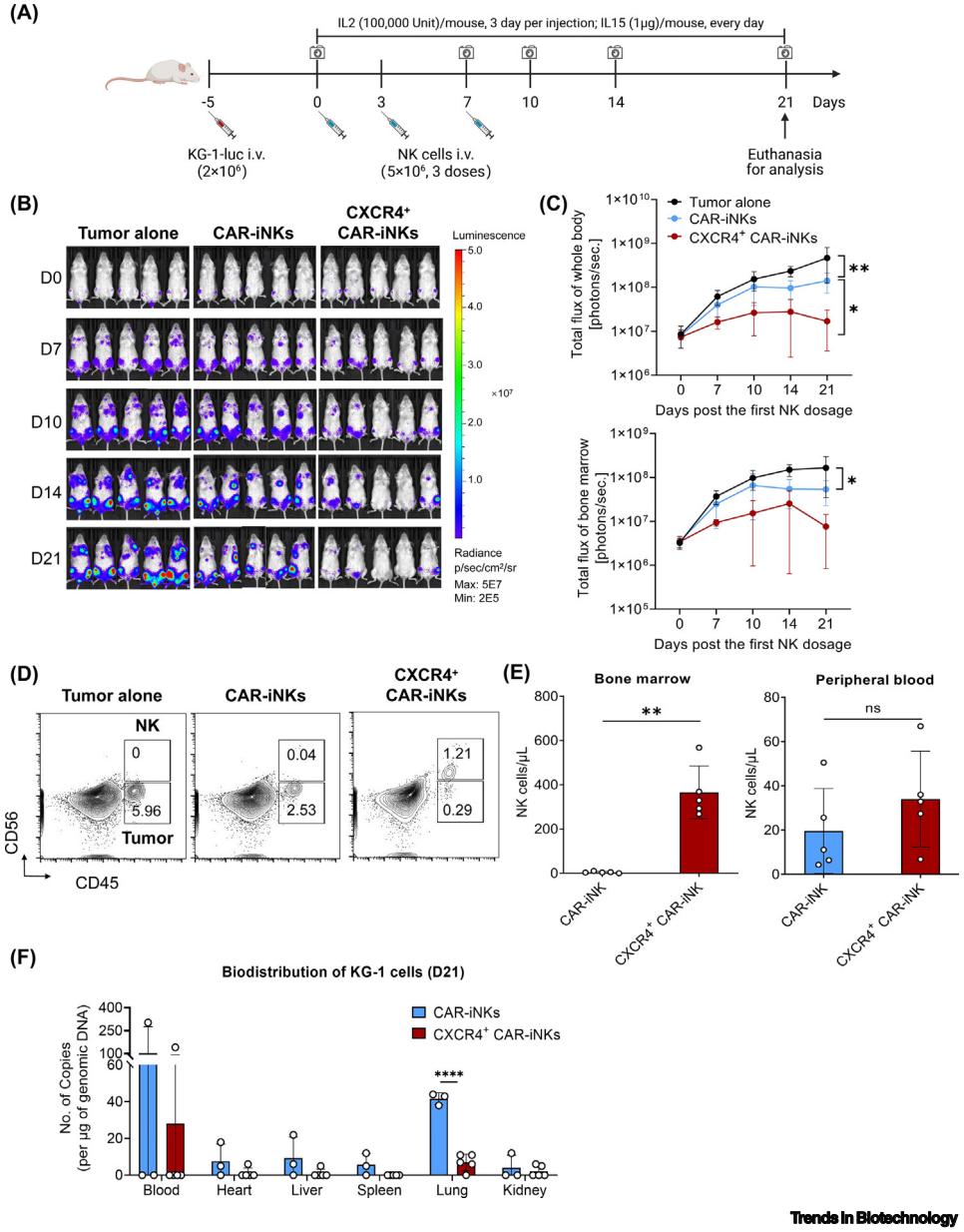


Figure 6. CXCR4$^+$ CAR-iNKs demonstrate enhanced BM homing and anti-AML potency. (A) Time schedule of *in vivo* antitumor function evaluation of CXCR4$^+$ CAR-iNKs using KG-1-luciferase xenograft models. (B) Tumor burden of each group in the KG-1-luc xenograft models monitored at the indicated time points. After tumor inoculation, mice were treated with CXCR4$^+$ CAR-iNKs ($n$ = 5) or CAR-iNKs ($n$ = 5). (C) Statistical analysis of total bioluminescence of whole body (up) and bone marrow (bottom). Differences between groups were determined using two-way ANOVA. (D) Flow cytometry analysis of human NK cells (gated on 'CD45$^+$CD56$^+$ population') and tumor cells (gated on 'CD45$^+$CD56$^-$ population') among tumor alone, CAR-iNKs, and CXCR4$^+$ CAR-iNKs group. (E) Distribution of iNKs in PB and BM (obtained from femur) detected at day 21. Technically, the cells extracted from PB and BM were resuspended in the same volume between CXCR4$^+$ CAR-iNKs and CAR-iNKs group. Left, unpaired $t$ test with Welch's correction; right, unpaired $t$ test. (F) Biodistributions of CAR-iNKs and CXCR4$^+$ CAR-iNKs in various tissues, including heart, liver, spleen, lung, kidney, and PB. Differences between groups were determined using Mann–Whitney $U$ test or unpaired $t$ test. Data are presented as mean ± SD (C,E,F). *$P$<0.05, **$P$<0.01, ****$P$<0.0001. Abbreviations: BM, bone marrow; CXCR4, C-X-C chemokine receptor type 4; GZMB, granzyme B; iNK, iPSC-derived natural killer cell; ns, no statistical significance; PB, peripheral blood.

iNK cell number in the CXCR4$^{+}$ CAR-iNK group (Figure S8C–E). Combining all these results, we concluded that CXCR4$^{GZMB}$ modification further boost *in vivo* efficacy of CAR-iNKs by enhancing BM homing, indicating a potential cell product with improved therapeutic effects on AML.

## Discussion

With the advancement of cell therapy, several immune cell products, such as Kymirah and Yescarta, have secured approval in succession. However, none of them are tailored for AML, underscoring a pressing and unmet medical need. AML is characterized by genetic mutations on HSCs, leading to abnormal myeloid cell production in the BM. Given that leukemia cells predominantly reside in the BM and subsequently circulate into the PB, the importance of ensuring cell products possess BM homing capabilities cannot be overstated. By modifying CAR-T and CAR-NK cells to ectopically express CXCR4 [21–26], enhanced BM infiltration and elimination of BM-resident AML cells have been demonstrated in xenograft mouse models, suggesting a promising strategy to improve efficacy through chemokine receptor modulation. Therefore, conducting a thorough evaluation of chemotaxis is imperative during the manufacturing process of cell products.

Recently, numerous clinical trials have investigated AML treatment, encompassing both CAR-T and CAR-NK cell therapies. Although CAR-T cell therapy has exhibited significant efficacy in tumor cell elimination and achieving high rates of complete remission, its broader application in AML has been hindered by notable adverse effects. Despite many researchers targeting CD33 and CLL1 due to their prevalence in AML, the persistent expansion of CAR-T cells has led to prolonged myelosuppressive effects, such as neutropenia and thrombocytopenia. Consequently, NK cells, including iNKs, are emerging as a promising cell type for AML therapy due to their intrinsic properties, as evidenced by several clinical studies [27,28]. Recent findings have indicated a significant decline in CXCR4 levels in PBNK cells during expansion, highlighting the necessity of incorporating CXCR4 into the evaluation system for the manufacturing process. Nonetheless, to date, there has been limited exploration of the chemokine pathway for enhancing NK cell or iNKs efficacy in AML.

Crucially, iNKs, with their potential for complex genetic engineering at iPSC stage, provide a stable and readily accessible product for various indications. Except when focusing on the expansion potential and cytotoxic capability of iNK, this study highlights the critical analysis of iNK chemotaxis. Interestingly, a notable disparity exists between PBNKs and iNKs in terms of *in vivo* trafficking and distribution (see Figure S9). Through this, more attention was brought to the chemotaxis of cell products, especially with an extended *in vitro* manufacturing process, and using iPSCs or other stem cells as the cell source.

To underscore the necessity, we observed marginal expression of CXCR4 in our iNKs, which cannot be attributed to the differentiation protocol. Despite attempting multiple publicly available protocols (data not shown) and engineering of iPSC with consistent CXCR4 expression, none yielded a distinct CXCR4$^{+}$ iNK population. With stepwise RNA-seq analysis, we revealed the underlying biological mechanism that CXCR4 delayed mesoderm formation and induced hematopoiesis failure. Additionally, research has indicated that impaired CXCR4 desensitization is linked with defective generation of lymphoid-committed progenitors in the BM [20]. Similarly, severe panleukopenia is observed in **WHIM syndrome**, caused by gain-of-function mutations in CXCR4 [29,30]. All of these findings highlight the essential role of appropriate CXCR4 retention and desensitization during the hematopoietic cell development and their differentiation towards T and NK cells, hinting at a critical avenue for iNK optimization.

To harness the advantages of CXCR4 in AML targeting, we devised a genetic engineering strategy to overcome the limitations of differentiation in terms of CXCR4 expression. Specifically, we

engineered iPSC with a targeted knock-in of the CXCR4 transgene at the GZMB locus and successfully obtained $CXCR4^{+}$ iNKs without compromising yield, expansion potential, and cytotoxicity against tumor cells. Remarkably, the $CXCR4^{GZMB}$ iNKs maintained stable CXCR4 expression throughout expansion, suggesting a potential method to enhance PBNK function through similar engineering. Unexpectedly, our attempts to integrate the CXCR4 transgene in a comparable manner at the NCR3 locus failed to yield $CXCR4^{+}$ iNKs (Figure S10), which might be attributed to alternative transcript splicing, as suggested by other studies [31], necessitating further elucidation in the future. Nevertheless, we provide a methodology for temporally regulating transgene expression to mitigate its impact on pluripotency maintenance, differentiation, and other critical aspects. In the context of cell-based product development, genetic engineering strategies are commonplace and should be thoughtfully designed to enhance function, particularly in the realm of iPSC-based cell therapy.

Furthermore, we evaluated the function of $CXCR4^{GZMB}$ iNKs both *in vitro* and *in vivo*. The heightened expression of CXCR4 significantly improved NK cell infiltration into BM, resulting in complete eradication of BM-resident tumor cells. Moreover, our further exploration of $CXCR4^{GZMB}$ iNK infiltration into other organs revealed no significant differences compared with the control group, indicating low safety concerns. Meanwhile, the absence of immune cell aggregation symptoms in other organs in patients with WHIM syndrome further suggested safety [32]. This opens the possibility of further augmenting CXCR4 chemotaxis through engineering with gain-of-function CXCR4 mutations, as demonstrated by the superior response to CXCL12 (Figure S11). Certainly, integrating CXCR4 into NK cells alongside other modifications, such as aCD33-CAR and aCLL1-CAR, to create the final cell product for AML warrants further evaluation of overall efficacy and safety in clinical conditions.

In conclusion, this study underscores the importance of *in vivo* distribution and chemotaxis profiling during cell product development, urging optimization of the manufacturing process accordingly. Regarding iNKs, we observed a lack of CXCR4 expression, resulting in limited BM homing. Further analysis revealed that constitutive CXCR4 modification on iPSC impacts their differentiation towards NK cells by disturbing the HSC formation. To overcome this limitation, we devised a novel strategy and demonstrated that CXCR4 knock-in at the GZMB locus is a feasible strategy to significantly enhance the chemotaxis of iNKs to the BM. Importantly, the engineered iNKs exhibited a substantial improvement in BM infiltration, leading to the complete eradication of BM-resident tumor cells. Incorporation of this strategy with CAR components deepens the therapeutic efficacy, suggesting a potential prototype for AML. This signifies a practical and promising avenue to advance cell-based therapy for AML.

## Concluding remarks

AML is a clonal hematopoietic stem cell malignancy characterized by the accumulation of immature myeloid blasts with arrested differentiation, resulting in hematopoietic suppression. Despite standard-of-care treatments, most patients experience relapse and have poor prognoses, with a median OS of only 6 months and a 5-year OS of 10%. Consequently, there is a high demand for potent therapeutics for relapsed or refractory AML (R/R AML). Cellular immunotherapy, such as CAR-T cell therapy, has shown promising initial clinical outcomes in AML patients, while being hampered by severe adverse effects. Recently, iNKs, iPSC-derived T cells (iTs), or iPSC-derived macrophages (iM) with various functional modules have displayed cytotoxicity against various tumor types, including AML. Despite numerous studies aiming to enhance their antitumor activity, there has been limited investigation into their *in vivo* chemotaxis, particularly to the BM. Research has indicated significant alterations in chemokine receptors during stem cell differentiation, highlighting the importance of proper monitoring differentiation process and characteristics of final products (see Outstanding questions).

## Outstanding questions

How can we utilize current knowledge and technology to develop cell-based therapies with minimal adverse effects and enhanced benefits for patients with R/R AML?

Given the widespread application of iPSC as a starting cell source, what strategies can be employed to regulate the differentiation process and implement quality control measures to produce efficacious cell products?

We observed a significant improvement in the efficacy of the final CAR-iNKs in treating AML. Can these findings be translated into clinical benefits? Are there additional components, such as elements to enhance persistence, that should be incorporated into the final product to further strengthen its efficacy?

In this study, we observed limited BM infiltration of iNKs and found a significant reduction in CXCR4 gene expression. However, iPSCs with constitutive CXCR4 expression were unable to differentiate into hematopoietic cells, as indicated by differentiation failure and the absence of $CXCR4^+$ iNKs. To address this limitation, the CRISPR/Cas9 system was employed to knock-in the CXCR4 gene at the GZMB locus, enabling CXCR4 expression specifically at the iNKs maturation stage without compromising the final yield and function of iNKs. The CXCR4-enhanced iNKs and CAR-iNKs demonstrated successful augmentation of BM infiltration capability, leading to improved therapeutic effects in AML mouse models. This highlights the importance of CXCR4 in mediating iNK BM chemotaxis and provides a strategic method involving precise genetic engineering to enhance the therapeutic effects of iNKs in AML, signifying a practical and promising avenue to advance cell-based therapy for AML. Meanwhile, this study demonstrated a good example of incorporating well-designed genetic engineering with stem cell differentiation for cell product development, providing a methodology for temporally regulating transgene expression to mitigate its impact on pluripotency maintenance, differentiation, and other critical aspects.

## STAR★METHODS

Detailed methods are provided in the online version of this paper and include the following:

- KEY RESOURCES TABLE
- EXPERIMENTAL MODEL AND STUDY PARTICIPANT DETAILS
  - Cell lines and cell culture
  - Mice
- METHOD DETAILS
  - Lentivirus production and titration
  - iNKs expansion and transduction
  - RNA-seq sample collection and data analysis
  - Generation of $CXCR4^{GZMB}$ and $BFP^{GZMB}$ iPSC clones
  - iNKs differentiation from engineered iPSC
  - iNKs phenotype analysis
  - *In vitro* cytotoxicity assay
  - Cell cycle assay
  - Animal experiments
- QUANTIFICATION AND STATISTICAL ANALYSIS

## RESOURCE AVAILABILITY

### Lead contact

Further information and requests for resources and reagents should be directed to and will be fulfilled by the lead contact, Luhan Yang (luhan.yang@qihanbio.com).

### Materials availability

This study did not generate new unique materials.

### Data and code availability

- All the original code has been deposited at Zenodo (https://zenodo.org/records/14740912).
- Any additional information required to reanalyze the data reported in this paper is available from the lead contact upon request.

#### Author contributions

X.H., L.W., W.Z., and Y.W. designed the project, developed the methodology, conducted experiments, validated assays, analyzed data, and contributed to manuscript writing. N.C., Q.Z., Y.S., and G.M. conducted animal experiments. P.Y., A.T., and Y.D. conducted bioinformatics analysis. M.W., Z.H., X.Z., M.X., L.L., X.W., X.D., T.Z., P.Z., Z.P., F.Y., Y.Z., J.H., Y.Y., and J.H. conducted molecular biology and function verification experiments. T.H., G.M.C., X.H., Y.H., H.H., and L.Y. jointly supervised this work. All authors reviewed and approved the final version of the manuscript.

## Acknowledgments

These studies received support from the National Natural Science Foundation of China (82341206, 82130003, and 31970774), and Key Project of Science and Technology Department of Zhejiang Province (2023C03060). We express our gratitude to the Yangtze Delta Region Institute of Tsinghua University, Zhejiang, Hangzhou, for their support at the site and oversight from the Ethics Committee. Schematic figures were created with BioRender.com.

## Declaration of interests

T.H. and G.M.C. are consultants and shareholders of Qihan Bio Inc. X.H., W.Z., N.C., P.Y., A.T., Q.Z., Y.S., M.W., M.X., L.L., X.W., X.D., T.Z., P.Z., Z.P., F.Y., Y.Z., G.M., J.H., Y.Y., J.H., and L.Y. are employed by Qihan Bio Inc., and L.Y. is the chief executive officer. Furthermore, we have a patent application related to this work. All remaining authors have no competing interests to declare.

## Supplemental information

Supplemental information associated with this article can be found online at https://doi.org/10.1016/j.tibtech.2025.02.018.

## References

1. Döhner, H. *et al.* (2015) Acute myeloid leukemia. *N. Engl. J. Med.* 373, 1136–1152
2. Döhner, H. *et al.* (2021) Towards precision medicine for AML. *Nat. Rev. Clin. Oncol.* 18, 577–590
3. Walter, R.B. (2024) Perspective on measurable residual disease testing in acute myeloid leukemia. *Leukemia* 38, 10–13
4. Ma, J. and Ge, Z. (2021) Recent advances of targeted therapy in relapsed/refractory acute myeloid leukemia. *Bosn. J. Basic Med. Sci.* 21, 409–421
5. Hu, Y. *et al.* (2022) CAR T-cell therapies in China: rapid evolution and a bright future. *Lancet Haematol.* 9, e930–e941
6. Hu, Y. *et al.* (2022) Genetically modified CD7-targeting allogeneic CAR-T cell therapy with enhanced efficacy for relapsed/refractory CD7-positive hematological malignancies: a phase I clinical study. *Cell Res.* 32, 995–1007
7. Stevens, B.M. *et al.* (2019) CD123 CAR T cells for the treatment of myelodysplastic syndrome. *Exp. Hematol.* 74, 52–63.e53
8. Jin, X. *et al.* (2022) First-in-human phase I study of CLL-1 CAR-T cells in adults with relapsed/refractory acute myeloid leukemia. *J. Hematol. Oncol.* 15, 88
9. Perna, F. *et al.* (2017) Integrating proteomics and transcriptomics for systematic combinatorial chimeric antigen receptor therapy of AML. *Cancer Cell* 32, 506–519.e505
10. Guillerey, C. *et al.* (2016) Targeting natural killer cells in cancer immunotherapy. *Nat. Immunol.* 17, 1025–1036
11. Knorr, D.A. *et al.* (2013) Clinical-scale derivation of natural killer cells from human pluripotent stem cells for cancer therapy. *Stem Cells Transl. Med.* 2, 274–283
12. Li, Y. *et al.* (2018) Human iPSC-derived natural killer cells engineered with chimeric antigen receptors enhance anti-tumor activity. *Cell Stem Cell* 23, 181–192.e185
13. Hermanson, D.L. *et al.* (2016) Induced pluripotent stem cell-derived natural killer cells for treatment of ovarian cancer. *Stem Cells* 34, 93–101
14. Saetersmoen, M.L. *et al.* (2019) Off-the-shelf cell therapy with induced pluripotent stem cell-derived natural killer cells. *Semin. Immunopathol.* 41, 59–68
15. Grzywacz, B. *et al.* (2019) Natural killer cell homing and persistence in the bone marrow after adoptive immunotherapy correlates with better leukemia control. *J. Immunother.* 42, 65–72
16. Ladikou, E.E. *et al.* (2020) Dissecting the role of the CXCL12/CXCR4 axis in acute myeloid leukaemia. *Br. J. Haematol.* 189, 815–825
17. Lasry, A. *et al.* (2023) An inflammatory state remodels the immune microenvironment and improves risk stratification in acute myeloid leukemia. *Nat. Cancer* 4, 27–42
18. Felker, S. *et al.* (2022) Differential CXCR4 expression on hematopoietic progenitor cells versus stem cells directs homing and engraftment. *JCI Insight* 7, e151847
19. Zou, Y. *et al.* (2014) Manipulating the expression of chemokine receptors enhances delivery and activity of cytokine-induced killer cells. *Br. J. Cancer* 110, 1992–1999
20. Freitas, C. *et al.* (2017) Lymphoid differentiation of hematopoietic stem cells requires efficient Cxcr4 desensitization. *J. Exp. Med.* 214, 2023–2040
21. Nian, Z. *et al.* (2021) Rapamycin pretreatment rescues the bone marrow AML cell elimination capacity of CAR-T cells. *Clin. Cancer Res.* 27, 6026–6038
22. Jamali, A. *et al.* (2020) Highly efficient generation of transgenically augmented CAR NK cells overexpressing CXCR4. *Front. Immunol.* 11, 2028
23. Levy, E. *et al.* (2019) Enhanced bone marrow homing of natural killer cells following mRNA transfection with gain-of-function variant CXCR4(R334X). *Front. Immunol.* 10, 1262
24. Ng, Y.Y. *et al.* (2022) CXCR4 and anti-BCMA CAR co-modified natural killer cells suppress multiple myeloma progression in a xenograft mouse model. *Cancer Gene Ther.* 29, 475–483
25. Segerberg, F. *et al.* (2023) Improved leukemia clearance after adoptive transfer of NK cells expressing the bone marrow homing receptor CXCR4(R334X). *Hemasphere* 7, e974
26. Arai, Y. *et al.* (2018) Myeloid conditioning with c-kit-targeted CAR-T cells enables donor stem cell engraftment. *Mol. Ther.* 26, 1181–1197
27. Cichocki, F. *et al.* (2020) iPSC-derived NK cells maintain high cytotoxicity and enhance in vivo tumor control in concert with T cells and anti-PD-1 therapy. *Sci. Transl. Med.* 12, eaaz5618
28. Chiu, E. *et al.* (2021) Anti-NKG2C/IL-15/anti-CD33 killer engager directs primary and iPSC-derived NKG2C(+) NK cells to target myeloid leukemia. *Mol. Ther.* 29, 3410–3421
29. Gao, J.L. *et al.* (2023) CRISPR/Cas9-mediated Cxcr4 disease allele inactivation for gene therapy in a mouse model of WHIM syndrome. *Blood* 142, 23–32
30. Balabanian, K. *et al.* (2012) Proper desensitization of CXCR4 is required for lymphocyte development and peripheral compartmentalization in mice. *Blood* 119, 5722–5730
31. Zhang, C. *et al.* (2018) Homology-independent multiallelic disruption via CRISPR/Cas9-based knock-in yields distinct functional outcomes in human cells. *BMC Biol.* 16, 151
32. Heusinkveld, L.E. *et al.* (2019) WHIM syndrome: from pathogenesis towards personalized medicine and cure. *J. Clin. Immunol.* 39, 532–556
33. Ng, E.S. *et al.* (2008) A protocol describing the use of a recombinant protein-based, animal product-free medium (APEL) for human embryonic stem cell differentiation as spin embryoid bodies. *Nat. Protoc.* 3, 768–776

## STAR★METHODS

### KEY RESOURCES TABLE

| Reagent or resource | Source | Identifier |
|---|---|---|
| Antibodies | | |
| Anti-human IL15-APC | Thermo Fisher Scientific | Cat#MA5-23627, RRID:AB_2608838 |
| Anti-human CXCR4-APC | Biolegend | Cat#306510, RRID:AB_314616 |
| Anti-human CXCR4-BV421 | Biolegend | Cat#306518, RRID:B354130 |
| Anti-human TRA-1-81-AF647 | BD Biosciences | Cat#560793, RRID:AB_10550550 |
| Anti-human SSEA-4-PE | BD Biosciences | Cat#560128, RRID:AB_1645533 |
| Anti-human CD34-APC | BD Biosciences | Cat#555824, RRID:AB_398614 |
| Anti-human CD43-FITC | BD Biosciences | Cat#555475, RRID:AB_395867 |
| Anti-human CD45-FITC | BD Biosciences | Cat#555482, RRID:AB_395874 |
| Anti-human CD56-APC | BD Biosciences | Cat#341026, RRID:AB_400559 |
| Anti-human CD94-PE | Thermo Fisher Scientific | Cat#12-0949-42, RRID:AB_10854417 |
| Anti-human Granzyme B-PB | Biolegend | Cat#515408 RRID: AB_2562196 |
| Anti-human CLL1-PE/Cyanine7 | Biolegend | Cat#353609 RRID:AB_2563671 |
| Anti-human CD33-APC | BD Biosciences | Cat#551378 RRID:AB_398502 |
| Anti-human MICA/B-PE | Thermo Fisher Scientific | Cat#12-5788-42, RRID:AB_10854117 |
| Anti-human ULBP1-PE | R&D Systems | Cat#FAB1380P, RRID:AB_2687471 |
| Anti-human ULBP2/5/6-PE | R&D Systems | Cat#FAB1298P, RRID:AB_2214693 |
| Anti-human ULBP3-PE | R&D Systems | Cat#FAB1517P, RRID:AB_10719122 |
| Anti-human ULBP4-PE | R&D Systems | Cat#FAB6285P RRID:AB_3083729 |
| PE Mouse IgG1 κ Isotype Control | BD Biosciences | Cat#555749, RRID:AB_396091 |
| FITC Mouse IgG1 κ Isotype Control | BD Biosciences | Cat#555748, RRID:AB_396090 |
| APC Mouse IgG1 κ Isotype Control | BD Biosciences | Cat#555751, RRID:AB_398613 |
| Bacterial and virus strains | | |
| TOP10 | Weidi Biotech | Cat#DL1010M |
| Chemicals, peptides, and recombinant proteins | | |
| StemFit Basic03 | Ajinomoto Co., Inc. | Cat#34770 |
| bFGF | PeproTech | Cat#191128A |
| Laminin 521 | Biolamina | Cat#CT521-0501 |
| DPBS | Gibco | Cat#A1285801 |
| Y-27632 | Stemcell | Cat#72308 |
| RPMI 1640 Medium | Gibco | Cat#11875093 |
| Dulbecco's Modified Eagle Medium (DMEM) | Gibco | Cat#10569010 |
| Fetal bovine serum (FBS) | Gibco | Cat#10100-147 |
| KBM581 media | Corning | Cat#88-581-CM |
| Human male AB serum | Access Biologicals | Cat#515 |

(continued)

| Reagent or resource | Source | Identifier |
|---|---|---|
| Phosphate buffered saline (PBS) | Gibco | Cat#10010-023 |
| Bovine serum albumin (BSA) | Sigma | Cat#A9543 |
| TrypLE Express | Gibco | Cat#12604-021 |
| 2-mercaptoethanol | Gibco | Cat#21985023 |
| Recombinant Human IL-2 | Beijing Four Rings Bio-Pharmaceutical Co., Ltd | Cat#20200714 |
| PEIpro | Polyplus | Cat#115-010 |
| Polybrene | Sigma | Cat#TR-1003-G |
| RetroNectin | TAKARA | Cat#T100A |
| Recombinant Human SDF-1α | PeproTech | Cat#300-28A |
| UltraPure™ DNase/RNase-Free Distilled Water | Invitrogen | Cat#10977015 |
| CS10 | Biolife Solutions Inc. | Cat#210502 |
| Cas9 Protein | Invitrogen | Cat#A36498 |
| Propidium iodide | Thermo Fisher Scientific | Cat#P3566 |
| FxCycle™ PI/RNase | Invitrogen | Cat#F10797 |
| Bright-Glo Luciferase assay system | Promega | Cat#E2610 |
| Clone R | Stemcell | Cat#05889 |
| Critical commercial assays | | |
| Human CXCL12/SDF-1 ELISA Kit | MultiSciences | Cat#EK1119-96 |
| P3 Primary Cell 4D-Nucleofector X Kit | Lonza | Cat#V4XP-3032 |
| Deposited data | | |
| N/A | N/A | N/A |
| Experimental models: cell lines | | |
| THP-1 | ATCC | Cat#TIB-202 |
| K562 | Mingzhou Biotech | Cat#MZ-0102 |
| KG-1 | ATCC | Cat#CRL-8031 |
| 293T | Hunan Fenghui Biotech | Cat#CL0005 |
| Human artificial antigen-presenting cells | Hangzhou Qihan Biotech | N/A |
| Human PBNK | Shanghai Saily Biotech | N/A |
| Experimental models: organisms/strains | | |
| Mouse: NOD.Cg-*Prkdc*$^{scid}$*Il2rg*$^{tm1Sug}$/JicCrl (NOG) | Beijing Vital River Laboratory Animal Technology | N/A |
| Mouse: NOD/ShiLtJGpt-*Prkdc*$^{em26Cd52}$*Il2rg*$^{em26Cd22}$/Gpt (NCG) | GemPharmatech | N/A |
| Oligonucleotides | | |
| Granzyme B sgRNA: 5 ′-AAGGTGTTTCATTACAGCGG-3′ | GenScript Biotech | Custom order |
| Granzyme B-junction PCR-LA-forward primer: 5′-GGGGCCCAGAAGTTCGTT-3′ | Tsingke Biotech | Custom order |
| Granzyme B-junction PCR-LA-reverse primer: 5′-GCCCTCGTTTTCGTAGCG-3′ | Tsingke Biotech | Custom order |
| NKP30-junction PCR-RA-forward primer: 5′-GCATCGCATTGTCTGAGTAGGT-3′ | Tsingke Biotech | Custom order |
| Granzyme B-junction PCR-RA-reverse primer: 5′-GTTTCACTTGGGTTCAGATG-3′ | Tsingke Biotech | Custom order |

*(continued on next page)*

(continued)

| Reagent or resource | Source | Identifier |
|---|---|---|
| Granzyme B-WT-forward primer: 5′-TGTGTAACAAGGTGGCCCAG-3′ | Tsingke Biotech | Custom order |
| Granzyme B-WT-reverse primer: 5′-CCCTGGAGAAACTGGTGTGG-3′ | Tsingke Biotech | Custom order |
| Backbone forward primer: 5′-ACGACGTGACCCTGTTCATC-3′ | Tsingke Biotech | Custom order |
| Backbone reverse primer: 5′-CCGCTTACCGGATACCTGTC-3′ | Tsingke Biotech | Custom order |
| hGAPDH-forward primer: 5′-CTCCCCACACACATGCACTTA-3′ | Tsingke Biotech | Custom order |
| hGAPDH-probe: 5′-AAAAGAGCTAGGAAGGACAGGCAACTTGGC-3′ | Tsingke Biotech | Custom order |
| hGAPDH-reverse primer: 5′-CCTAGTCCCAGGGCTTTGATT-3′ | Tsingke Biotech | Custom order |
| BFP-forward primer: 5′-AGACCTTCATCAACCACACCC-3′ | Tsingke Biotech | Custom order |
| BFP-probe: 5′-GCATGACTGGTCCATTAGAGGT-3′ | Tsingke Biotech | Custom order |
| BFP-reverse primer: 5′-TGGAGGTGTGTTGACTGCTACCCA-3′ | Tsingke Biotech | Custom order |
| CXCR4-forward primer: 5′-GCTGTTGGCTGAAAAGGTGG-3′ | Tsingke Biotech | Custom order |
| CXCR4-probe: 5′-TGGCGTCTGGATCCCTGCCCTCCTGCTGAC-3′ | Tsingke Biotech | Custom order |
| CXCR4-reverse primer: 5′-ATCTGCCTCACTGACGTTGG-3′ | Tsingke Biotech | Custom order |
| Granzyme B-FA-forward primer: 5′-CCTCTTGTGTGTAACAAGGT-3′ | Tsingke Biotech | Custom order |
| Granzyme B-FA-reverse primer: 5′-ACCTCTCCCAGTGTAAATCT-3′ | Tsingke Biotech | Custom order |
| Recombinant DNA | | |
| CXCR4 construct | This manuscript | N/A |
| Truncated CXCR4 construct | This manuscript | N/A |
| Anti-CD33 scFv | This manuscript | N/A |
| Anti-CLL1 scFv | This manuscript | N/A |
| Software and algorithms | | |
| Graphpad Prism v9.0 | GraphPad software | https://www.graphpad.com |
| FlowJo v10.0 | FlowJo, LLC | https://www.flowjo.com/ |
| Incucyte Base Software | Sartorius | https://www.sartorius.com/en/products/live-cell-imaging-analysis/live-cell-analysis-software |
| R version v4.2.1 | R Core Team 2017 | https://www.r-project.org |
| Fastqc v0.11.8 | Software | https://www.bioinformatics.babraham.ac.uk/projects/fastqc/ |
| Fastp v0.20.0 | Software | https://github.com/OpenGene/fastp |
| Salmon v0.14.1 | Software | https://doi.org/10.1038/nmeth.4197 |
| Tximport v1.34.0 | R package | https://bioconductor.org/packages/release/bioc/html/tximport.html |

(continued)

| Reagent or resource | Source | Identifier |
|---|---|---|
| Heatmaps v1.30.0 | R package | https://bioconductor.org/packages/release/bioc/html/heatmaps.html |
| ClusterProfiler v4.14.3 | R package | https://www.bioconductor.org/packages/release/bioc/html/clusterProfiler.html |
| EMBL EBI GO database | QuickGO | QuickGO::Annotation List |

## EXPERIMENTAL MODEL AND STUDY PARTICIPANT DETAILS

### Cell lines and cell culture

THP-1 and KG-1 cell lines were purchased from ATCC (Manassas VA USA), and K562 was purchased from Mingzhou Biotech. These tumor cell lines were subsequently genetically modified to stably express luciferase and GFP for *in vitro* and *in vivo* assays. THP-1, KG-1, and K562 cells were cultured in RPMI 1640 medium (Gibco) supplemented with 10% fetal bovine serum (Gibco). Furthermore, 2-mercaptoethanol (Gibco) was incorporated into the THP-1 culture medium at a final concentration of 0.05 mM.

### Mice

Female NOG or NCG mice aged 6-8 weeks were used in this study. To establish a mouse xenograft model of AML, THP-1 and KG-1 cells labeled with luciferase were intravenously injected via the tail vein. Subsequently, the mice were randomized into different treatment groups. Starting on day 3 or 5 after tumor inoculation, the mice were intravenously administered with iNKs or CXCR4 overexpression iNKs. Tumor growth was monitored using bioluminescence imaging (BLI), and data acquisition and analysis were performed using Xenogen Living Imaging software v2.5. Peripheral blood and bone marrow samples from the femur were collected from euthanized mice to analyze the biodistribution of iNKs via flow cytometry detecting CD56. To assure the uniformity, *ex vivo* bone marrow was resuspended by 200μL PBS for further analysis. Various tissues were collected as well for pharmacokinetic analysis. All studies were approved by the Yangtze Delta Region Institute of Tsinghua University, Zhejiang, Hangzhou.

## METHOD DETAILS

### Lentivirus production and titration

The lentiviral vector (encoding CXCR4 or luciferase) was generated by transiently transfecting 293T cells with gag-pol and VSV-G packaging plasmids. The viral vector was harvested 48 hours and 60 hours post-transfection, respectively, then filtered (0.45 μm; Millipore) and incubated with PEG 6000 overnight at 4°C. After centrifugation at 2500g for 1 hour at 4°C, it was reconstituted in NK culture media. To determine the virus titration, 293T cells were seeded in 24-well plates at $1\times10^5$ cells per well. Titrated virus was added and supplemented with polybrene (Sigma) at a final concentration of 8 μg/ml. The titer was calculated by flow cytometry analysis 48 hours after transfection.

### iNKs expansion and transduction

K562 cell lines engineered with membrane-bound interleukin 21 and 4-1BBL were irradiated as artificial antigen-presenting cells (aAPCs) for stimulating the expansion of iNKs. Thawed iNKs were incubated with aAPCs for expansion at a 1:1 ratio in KBM581 media (Corning) supplemented with 10% human male AB serum (Access Biologicals) and 200 IU/ml IL2 for 4 days. Then, expanded iNKs were transferred to a 96-well plate precoated with virus at a concentration of $2\times10^5$ cells per well. To prepare the virus-precoated plate, RetroNectin reagent was used following the manufacturer's instructions (TAKARA), and virus particles were incubated at the indicated multiplicities of infection (MOIs). During transduction, polybrene (Sigma) was supplemented with a final concentration of 8 μg/ml. Spinoculation was performed at 1000g for 1 hour at 32°C, followed by transfer to the incubator for culture. After 24 hours, the transduced iNKs were expanded to obtain a sufficient cell number for *in vitro* and *in vivo* studies.

### RNA-seq sample collection and data analysis

Control iPSCs and $CXCR4^{high}$ iPSCs were prepared for iNK differentiation, and cell palette were collected at day 0, 3, and 9 of EB formation. Gene expression analyses were performed using Illumina PE250. Gene expression data were quantile-normalized and subsequently analyzed using salmon package. Differentially regulated genes were called using DESeq2 (Wald Test /Likelihood

Ratio Test). Differential expression thresholds were set to $\log_2$-fold change ≥1.5 (upregulated) or ≤1.5 (downregulated) with an adjusted *p*-value of ≤0.05 (corrected with Benjamini Hochberg equation). Heatmap clustering analysis and generation of GO-based heatmaps were performed in R package heatmap. The gene sets used in the heatmap were collected through EMBL EBI GO database (QuickGO). Gene set enrichment analysis (GSEA) was performed using clusterProfiler v4.14.3. GO analysis of biological processes based on The Human Gene Atlas were conducted using DAVID (DAVID Functional Annotation Tools).

### Generation of $CXCR4^{GZMB}$ and $BFP^{GZMB}$ iPSC clones

Utilizing a specific sgRNA, CRISPR/Cas9 induced a double-strand break at the GZMB 3' UTR locus, while simultaneously delivering a donor plasmid containing the integration cassette with anchored homology arms for repair. This procedure was conducted using a Lonza electroporator (Lonza, Chiba, USA). One week later, stable integration of iPSC cells, evidenced by GFP positivity, were sorted, followed by CRE transfection to excise the GFP-expressing element. Three days thereafter, GFP-negative iPSCs were sorted into 96-well plates using a SONY SH800S cell sorter for single clone growth and screening. To confirm correct transgene integration, genomic DNA was isolated from the iPSCs, followed by junction PCR and ddPCR analyses.

### iNKs differentiation from engineered iPSC

Human iPSC were cultured in StemFit Basic03 medium (Ajinomoto) supplemented with human bFGF on laminin-521 (LN-521)-coated plates. The differentiation method of NK cells from iPSC has been previously described, which includes embryonic formation, NK cell differentiation and NK cell expansion [11,33]. The expansion of differentiated NK cells was stimulated by aAPCs as mentioned above. The purity and transgene expression of expanded iNKs were tested before functional assay.

### iNKs phenotype analysis

The following monoclonal antibodies conjugated to PE, APC, FITC, or PB were used: TRA-1-81 (BD Biosciences), SSEA-4 (BD Biosciences), CD34 (BD Biosciences), CD43 (BD Biosciences), CD56 (BD Biosciences), CXCR4 (Biolegend), MICA/B (Thermo Fisher Scientific), ULBP1 (R&D Systems), ULBP2/5/6 (R&D Systems), ULBP3 (R&D Systems), and ULBP4 (R&D Systems). All antibodies were applied for a 20-minute staining period at room temperature and protected from light. Subsequently, stained cells were washed, resuspended in buffer (1% BSA in PBS), and subjected to flow cytometry acquisition using a CytoFLEX S flow cytometer (BD Biosciences).

### *In vitro* cytotoxicity assay

To detect the cytotoxicity of iNKs, they were co-cultured with GFP-labeled target tumor cells at the specific Effector-to-Target (E:T) ratio, and the green fluorescence was monitored using the IncuCyte® S3 system every 3 hours. The green fluorescence data were normalized to that of the tumor cell monoculture to calculate cytotoxicity of iNKs.

### Cell cycle assay

The $1\times10^6$ NK cells were seeded in 12-well plates with 1 ml medium. After 4 or 24 hours incubation, cells were collected, washed with PBS, and fixed overnight with 75% ethanol at 4°C. In the following day, the cells were washed and hydrated with PBS, and stained with FxCycle™ PI/RNase (Invitrogen) for 30 minutes at room temperature in the dark. Finally, the fluorescence of cell suspension was detected using a CytoFLEX S flow cytometer (BD Biosciences), and FlowJo v10 was used for data processing.

### Animal experiments

Female NOG mice aged 6–8 weeks were used in this study. To establish a mouse xenograft model of AML, THP-1 or KG-1 cells labeled with luciferase were intravenously injected via the tail vein. Subsequently, the mice were randomized into different treatment groups. Starting on day 3 or 5 after tumor inoculation, the mice were intravenously administered with iNKs or CXCR4 overexpressed iNKs. Tumor growth was monitored using bioluminescence imaging (BLI), and data acquisition and analysis were performed using Xenogen Living Imaging software v2.5. Peripheral blood and bone marrow samples from the femur were collected from euthanized mice to analyze the biodistribution of iNKs via flow cytometry detecting CD56. To assure the uniformity, *ex vivo* bone marrow was resuspended by 200 µl PBS for further analysis. Various tissues were collected as well for pharmacokinetic analysis. All studies were approved by the Yangtze Delta Region Institute of Tsinghua University, Zhejiang, Hangzhou.

## QUANTIFICATION AND STATISTICAL ANALYSIS

Continuous variables are presented as the mean ± standard deviation. Normality and homogeneity of variance are analyzed to choose the suitable methods of statistics. Normality of all data was assessed via the Shapiro-Wilk normality test. Differences between two groups were calculated via either the Mann–Whitney *U* test or the unpaired t test, while comparisons among multiple groups were conducted using one-way ANOVA or Kruskal–Wallis analysis. Furthermore, cohorts with limited number of sample ($n < 3$) were excluded for statistical analysis owing to low statistical power. Survival data were illustrated using Kaplan–Meier curves, and differences were determined using log-rank test. Data stratified by two independent categorical variables were analyzed using two-way ANOVA. All statistical analyses were performed using GraphPad Prism 9, and $p$-value $< 0.05$ was considered indicative of statistical significance.